Journal of Ship Research, Vol. 39, No. 4, Dec. 1995, pp. 347–356

Nonlinear Studies of Dynamic Stability of Submarines in the Dive Plane

Fotis A. Papoulias[1] and **Harilaos A. Papadimitriou**[2]

The problem of dynamic stability of submersible vehicles in the dive plane is examined utilizing linear and nonlinear methods. Local bifurcations are studied with the means of perturbation and linearization techniques. The primary mechanism of loss of stability is identified in the form of generic Hopf bifurcations to periodic solutions. Stability of the resulting limit cycles is established using center manifold approximations and integral averaging. Particular emphasis is placed on analyzing the effects of the quadratic drag forces due to their crucial role on stability of periodic solutions. The methods described in this work could lead to techniques resulting in enlargement of the submerged operational envelope of a vehicle.

1. Introduction

THE DYNAMIC response of a submersible vehicle operating at the extremes of its operational envelope is becoming increasingly important in order to enhance vehicle operations. Traditionally, dynamic stability of motion is studied using eigenvalue analysis where the equations of motion are linearized around nominal straight-line level flight paths (Arentzen & Mandel 1960, Clayton & Bishop 1982, Feldman 1987). Under certain simplified assumptions, a simple criterion $G_v > 0$ can be obtained where the stability index G_v is function of the hydrodynamic coefficients in heave and pitch. Values for the stability index can be computed by

$$G_v = 1 - \frac{M_w(Z_q + m)}{Z_w M_q} \tag{1}$$

This index is analogous to the familiar stability coefficient for horizontal plane maneuvering and can be thought of as a high-speed approximation where the effect of the metacentric restoring moment is minimal. If the value of G_v is greater than zero, the vehicle is dynamically stable. As we point out in the next section, though, this is only a sufficient and rather conservative condition for stability. It is not a necessary condition in the sense that $G_v < 0$ indicates instability at infinite forward speed. It is quite possible that at normal operating speeds the vehicle might be directionally stable. Furthermore, $G_v < 0$ indicates a divergent loss of stability which is quite uncommon in the vertical plane. Most modern submarines exhibit a flutter-like instability at high speed, which cannot be analyzed using the above simplified index. Divergent motions may develop in combined six degrees of freedom (Papoulias et al 1993) and their occurrence cannot be analyzed by a single stability index.

In this work we examine the problem of stability of motion with controls fixed in the vertical plane, with particular emphasis on the mechanism of loss of stability of straight-line motion. We concentrate on open-loop conditions, since the closed-loop control problem has been previously analyzed (Papoulias et al 1995). The surge equation is decoupled from heave/pitch through a perturbation series approach (Bender & Orszag 1978). It is shown that loss of stability occurs in the form of generic bifurcations to periodic solutions (Guckenheimer & Holmes 1983). Taylor expansions and center manifold approximations are employed in order to isolate the main nonlinear terms that influence system response after the initial loss of stability (Hassard & Wan 1978). Integral averaging is performed in order to combine the nonlinear terms into a design stability coefficient (Chow & Mallet-Paret 1977). Special attention is paid to the study of the quadratic drag terms as they constitute some of the main nonlinear terms of the equations of motion. The difficulty associated with the nonsmoothness of the absolute value nonlinearities is dealt with by employing the concept of generalized gradient (Clarke 1983). This has the advantage of keeping the linear terms constant, unlike the linear/cubic approximation typically used in ship roll motion studies (Dalzell 1978), where the linear damping coefficient is a function of the assumed amplitude of motion.

Vehicle modeling in this work follows standard notation (Gertler & Hagen 1976, Smith et al 1978), and numerical results are presented for the DARPA SUBOFF model (Roddy 1990) for which a set of hydrodynamic coefficients and geometric properties is available. Furthermore, the baseline vehicle is marginally stable with controls fixed under normal operating conditions and can serve as a prime example for the techniques described in this work. The model has been experimentally validated for angles of attack on the hull between ±15 deg while the constant coefficient approximation introduces very little error in time-domain simulations (Tinker 1978).

Unless otherwise mentioned, all results in this work are presented in standard dimensionless form with respect to the vehicle length ℓ = 4.26 m, and nominal forward speed U = 2.44 m/s. All angular deflections are shown in degrees.

2. Problem formulation

Equations of motion

Assuming that vehicle motion is restricted in the vertical plane, the mathematical model consists of the coupled nonlinear heave and pitch equations of motion. In a moving coordinate frame fixed at the vehicle's geometrical center, Newton's equations of motion for a port/starboard symmetric and

[1]Associate professor, Department of Mechanical Engineering, Naval Postgraduate School, Monterey, California.
[2]Lieutenant, Hellenic Navy, Athens, Greece.
Manuscript received at SNAME headquarters October 1994; revised manuscript received August 17, 1995.

neutrally buoyant vehicle are expressed in dimensionless form as

$$m(\dot{w} - uq - z_G q^2 - x_G \dot{q}) = Z_{\dot{q}} \dot{q} + Z_{\dot{w}} \dot{w} + Z_q q + Z_w w - C_D \int_{\text{tail}}^{\text{nose}} b(x)(w - xq)\,|w - xq|\,dx + Z_\delta \delta \quad (2)$$

$$I_y \dot{q} + mz_G(\dot{u} + wq) - mx_G(\dot{w} - uq) = M_{\dot{q}} \dot{q} + M_{\dot{w}} \dot{w} + M_q q + M_w w + C_D \int_{\text{tail}}^{\text{nosc}} b(x)(w - xq)\,|w - xq|\,x\,dx - x_{GB} W\cos\theta - z_{GB} W\sin\theta + M_\delta \delta \quad (3)$$

where $x_{GB} = x_G - x_B$, $z_{GB} = z_G - z_B$, and the rest of the symbols are based on standard notation and are explained in the Nomenclature. Without loss of generality we can assume that $z_B = x_B = 0$, so that $x_{GB} = x_G$ and $z_{GB} = z_G$. The cross-flow integral terms in these equations become very important for high-angle-of-attack maneuvering, where they provide the primary motion damping. The drag coefficient, C_D, is assumed to be constant throughout the vehicle length for simplicity. This does not affect the qualitative properties of the results that follow. The vehicle pitch rate is

$$\dot{\theta} = q \quad (4)$$

Dynamic coupling between surge and heave/pitch is present due to coordinate coupling as a result of the nonzero metacentric height. Therefore, pitch and heave motions must be studied together with surge

$$m\dot{u} + mwq - mx_G q^2 + mz_G \dot{q} = X_{qq} q^2 + X_{\dot{u}} \dot{u} + X_{wq} wq + X_{ww} w^2 + X_{uu} u^2 + X_{nn} n^2 + X_{\delta\delta} \delta^2 \quad (5)$$

where we assume that both resistance and propulsive forces are proportional to the square of the speed or the propeller revolutions, respectively.

In analyzing controls fixed stability of motion, the case $\delta = 0$ is examined first. The steady-state solutions of the equations are determined by $\dot{w} = \dot{q} = \dot{u} = \dot{\theta} = q_0 = 0$, where subscript 0 indicates variable value at steady state. Substituting these conditions in (2) we get

$$Z_w w_0 - C_D A_w w_0\,|w_0| = 0 \quad (6)$$

where

$$A_w = \int_{\text{tail}}^{\text{nose}} b(x)dx \quad (7)$$

is the "waterplane" area. Since $Z_w < 0$, equation (7) admits only one solution, namely $w_0 = 0$. Equation (3) then yields

$$\tan\theta_0 = -\frac{x_{GB}}{z_{GB}} \quad (8)$$

while (5) is used to determine the nominal forward speed, u_0.

Reduction of order

The linearized surge, heave, and pitch equations of motion in the vicinity of the nominal point are

$$(m - X_{\dot{u}})\dot{u} + mz_G \dot{q} = 2X_{uu} u \quad (9)$$

$$(m - Z_{\dot{w}})\dot{w} - (mx_G + Z_{\dot{q}}) = (Z_q + m)q + Z_w w \quad (10)$$

$$(I_y - M_{\dot{q}})\dot{q} + mz_G \dot{u} - (mx_G + M_{\dot{w}})\dot{w} = M_w w + (M_q - mx_G)\,q + M_\theta \theta \quad (11)$$

where

$$M_\theta = x_{GB} W\sin\theta_0 - z_{GB} W\cos\theta_0 \quad (12)$$

is the hydrostatic restoring moment coefficient. The characteristic equation of (4), (9), (10), and (11) is obtained as

$$(-A_1\lambda + B_1)(A_2\lambda^3 + B_2\lambda^2 + C_2\lambda + D_2) + A_3\lambda^4 + B_3\lambda^3 = 0 \quad (13)$$

where

$$A_1 = m - X_{\dot{u}}$$

$$B_1 = 2X_{uu}$$

$$A_2 = (m - Z_{\dot{w}})(I_y - M_{\dot{q}}) - (Z_{\dot{q}} + mx_G)(M_{\dot{w}} + mx_G)$$

$$B_2 = -Z_w(I_y - M_{\dot{q}}) - (m - Z_{\dot{w}})(M_q - mx_G) - (Z_q + m)(M_{\dot{w}} + mx_G) - M_w(Z_{\dot{q}} + mx_G)$$

$$C_2 = -M_\theta(m - Z_{\dot{w}}) + Z_w(M_q - mx_G) - M_w(Z_q + m)$$

$$D_2 = M_\theta Z_w$$

$$A_3 = (mz_G)^2(m - Z_{\dot{w}})$$

$$B_3 = -(mz_G)^2 Z_w$$

It can be seen that the parameter (mz_G) is responsible for surge and heave/pitch coupling. For $z_G = 0$, equation (13) decouples into the surge eigenvalue $\lambda = B_1/A_1$ and the classical cubic characteristic equation for the vertical plane. It should be mentioned that the effect of the forward speed u is embedded into the definition for the dimensionless vehicle weight W through

$$W \rightarrow \frac{W}{\frac{1}{2}\rho u^2 L^2} \quad (14)$$

If we introduce a smallness parameter

$$\varepsilon = (mz_G)^2 \quad (15)$$

we can rewrite (13) in the form

$$(A + \varepsilon\alpha)\lambda^4 + (B + \varepsilon\beta)\lambda^3 + C\lambda^2 + D\lambda + E = 0 \quad (16)$$

where in terms of previously defined coefficients

$$A = -A_1 a_2$$

$$B = -A_1 B_2 + B_1 A_2$$

$$C = -A_1 C_2 + B_1 B_2$$

$$D = -A_1 D_2 + B_1 C_2$$

$$E = B_1 D_2$$

$$\alpha = m - Z_{\dot{w}}$$

$$\beta = -Z_w$$

Following Bender & Orszag (1978) we expand the solutions of (16) in a regular perturbation series

$$\lambda = \lambda_0 + \lambda_1 \varepsilon + O(\varepsilon^2) \quad (17)$$

where λ_0 is an eigenvalue for $\varepsilon = 0$ (uncoupled surge or heave/pitch), λ_1 is the first-order correction due to dynamic coupling, and $O(\varepsilon^2)$ contains second- and higher-order terms in ε. Substituting (17) into (16) we can get

$$\lambda = \lambda_0 - \frac{\lambda_0^3(\alpha\lambda_0 + \beta)}{4A\lambda_0^3 + 3B\lambda_0^2 + 2C\lambda_0 + D}\varepsilon + O(\varepsilon^2) \quad (18)$$

It can be seen that the correction term is very small compared with the uncoupled root as evidenced by the λ_0^3 term.

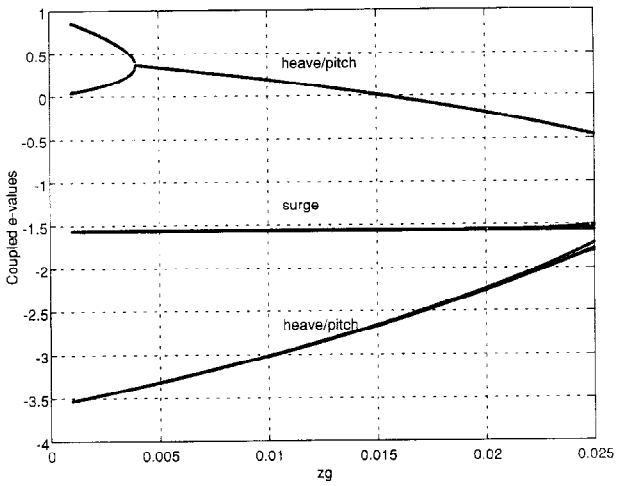

Fig. 1 System eigenvalues versus z_G

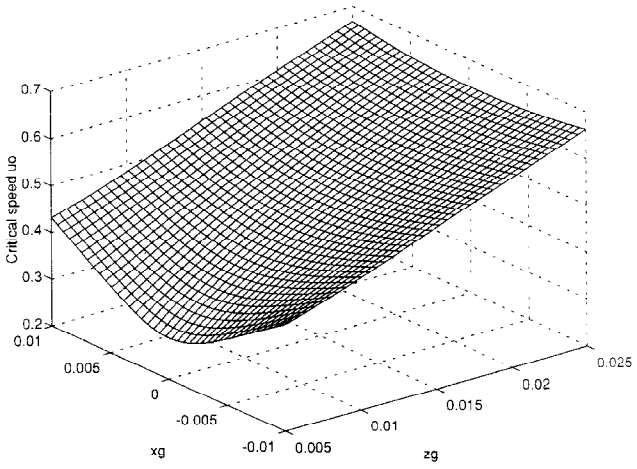

Fig. 2 Critical speed u_c versus x_G and z_G

This is particularly true when λ_0 nears zero, i.e., close to a bifurcation point. Therefore, loss of stability can be studied by analyzing the heave/pitch equations decoupled from surge. The characteristic equation then becomes

$$A_2\lambda^3 + B_2\lambda^2 + C_2\lambda + D_2 = 0 \tag{19}$$

A plot of the system eigenvalues at nominal speed versus z_G is shown in Fig. 1. The surge eigenvalues are real negative throughout the range of z_G, while the heave/pitch eigenvalues are real for small values of z_G. The two larger real heave/pitch eigenvalues coalesce into a complex conjugate pair whose real part crosses zero for a certain value of z_G. Within the accuracy of the graph, the eigenvalues λ are identical to those computed by either the coupled or the uncoupled system, or the perturbation equations (18).

Critical speed

The parameter value where the real part of the complex conjugate pair of eigenvalues shown in Fig. 1 crosses zero defines the point where linear stability is lost. This critical point can be computed by considering equation (19). Routh's criterion applied to this cubic yields $A_2D_2 = B_2C_2$ which can be solved for the dimensionless weight

$$W = \frac{B_2C_{2,0}}{A_2D_{2,1} - B_2C_{2,1}} \tag{20}$$

where

$$C_{2,0} = Z_w(M_q - mx_G) - M_w(Z_q + m)$$

$$C_{2,1} = (m - Z_{\dot{w}})(z_{GB}\cos\theta_0 - x_{GB}\sin\theta_0)$$

$$D_{2,1} = Z_w(x_{GB}\sin\theta_0 - z_{GB}\cos\theta_0)$$

The value of the critical speed u_c can then be evaluated from (20) and (14). Typical results are presented in Fig. 2, nondimensionalized with respect to nominal vehicle speed 2.44 m/s and length 4.26 m. Vertical plane motions are stable for forward speeds less than the critical speed. It can be seen that stability is increasing with increasing z_G while $x_G = 0$ is the most conservative condition for stability. Therefore, a vehicle which is stable when properly trimmed will remain stable for off-trim conditions. For comparison, we note that the simple stability coefficient G_v is monotonically decreasing and becomes more negative for decreasing x_G. Thus it would have predicted unstable motions for the entire range of parameters shown in Fig. 2.

3. Bifurcation analysis

Introduction

In all cases of stability loss of the previous section, one pair of complex conjugate eigenvalues of the corresponding eigenvalue problem crosses transversally the imaginary axis. A situation like this, in which a certain parameter is varied such that the real part of one pair of complex conjugate eigen-

Nomenclature

a = dummy independent variable
a_0 = steady-state value of a
α_{ij} = expansion coefficients of z_3 in terms of z_1, z_2
$b(x)$ = local beam of the hull
C_D = quadratic drag coefficient
γ = regularization parameter
δ = stern plane deflection
ε = perturbation parameter, $\varepsilon = (mz_G^2)$
ϵ = criticality difference, $\epsilon = u - u_c$
I_y = vehicle mass moment of inertia
K = nonlinear stability coefficient
LCB = longitudinal center of buoyancy
LCG = longitudinal center of gravity
λ = system eigenvalue
m = vehicle mass
M = pitch moment
M_a = derivative of M with respect to a
q = pitch rate
(R,ϕ) = polar coordinates of z_1, z_2
$\mathbf{T}$ = transformation matrix of $\mathbf{x}$ to $\mathbf{z}$
θ = pitch angle
u = forward speed
u_c = critical value of u
w = heave velocity
$\mathbf{x}$ = state variables vector, $\mathbf{x} = [\theta, w, q]$
X = surge force
X_a = derivative of X with respect to a
(x_B, z_B) = body fixed coordinates of vehicle center of buoyancy
(x_G, z_G) = body fixed coordinates of vehicle center of gravity
x_{GB} = center of gravity/center of buoyancy separation, $x_G - x_B$
z_{GB} = vehicle metacentric height, $z_G - z_B$
$\mathbf{z}$ = state variables vector in its normal form
z_1, z_2 = critical coordinates of $\mathbf{z}$
z_3 = stable coordinate of $\mathbf{z}$
Z = heave force
Z_a = derivative of Z with respect to a
ω_0 = imaginary part of critical pair of eigenvalues

values of the linearized system matrix crosses zero, results in the system leaving its steady state in an oscillatory manner. This loss of stability is called Hopf bifurcation and generally occurs in either supercritical or subcritical form. In the supercritical case, stable limit cycles are generated after the nominal straight-line motion loses its stability. The amplitudes of these limit cycles are continuously increasing as the parameter distance from its critical value is increased. For small values of this criticality distance the resulting limit cycle is of small amplitude and differs little from the initial nominal state. In the subcritical case, however, stable limit cycles are generated before the nominal state loses its stability. Therefore, depending on the initial conditions it is possible to diverge away from the nominal straight-line path and converge towards a limit cycle even before the nominal motion loses its stability. This means that in the subcritical Hopf bifurcation case the domain of attraction of the nominal state is decreasing and, in fact, it shrinks to zero as the critical point is approached. Random external disturbances of sufficient magnitude can throw the vehicle off to an oscillatory steady state even though the nominal state may still remain stable. After the nominal state becomes unstable, a discontinuous increase in the magnitude of motions is observed as there exist no simple stable nearby attractors for the vehicle to converge to. Distinction between these two qualitatively different types of bifurcation is, therefore, essential in design. The computational procedure requires higher-order approximations in the equations of motion and is the subject of this section.

Center manifold expansions

The nonlinear heave/pitch equations of motion (2), (3), and (4) are written in the form

$$\dot{\theta} = q \tag{21}$$

$$\dot{w} = a_{11}w + a_{12}q + a_{13}(x_{GB}\cos\theta + z_{GB}\sin\theta) + d_w(w,q) + c_1(w,q) \tag{22}$$

$$\dot{q} = a_{21}w + a_{22}q + a_{23}(x_{GB}\cos\theta + z_{GB}\sin\theta) + d_q(w,q) + c_2(w,q) \tag{23}$$

where

$$\begin{aligned}
D_v &= (m - Z_{\dot{w}})(I_y - M_{\dot{q}}) - (mx_G + Z_{\dot{q}})(mx_G + M_{\dot{w}}) \\
a_{11}D_v &= (I_y - M_{\dot{q}})Z_w + (mx_G + Z_{\dot{q}})M_w \\
a_{12}D_v &= (I_y - M_{\dot{q}})(m + Z_q) + (mx_G + Z_{\dot{q}})(M_q - mx_G) \\
a_{13}D_v &= -(mx_G + Z_{\dot{q}})W \\
a_{21}D_v &= (m - Z_{\dot{w}})M_w + (mx_G + M_{\dot{w}})Z_w \\
a_{22}D_v &= (m - Z_{\dot{w}})(M_q - mx_G) + (mx_G + M_{\dot{w}})(m + Z_q) \\
a_{23}D_v &= -(m - Z_{\dot{w}})W \\
d_w(w,q)D_v &= (I_y - M_{\dot{q}})I_w + (mx_G + Z_{\dot{q}})I_q \\
d_q(w,q)D_v &= (m - Z_{\dot{w}})I_q + (mx_G + M_w)I_w \\
c_1(w,q)D_v &= (I_y - M_{\dot{q}})mz_Gq^2 - (mx_G + Z_{\dot{q}})mz_Gwq \\
c_2(w,q)D_v &= -(m - Z_{\dot{w}})mz_Gwq + (mx_G + M_{\dot{w}})mz_Gq^2
\end{aligned}$$

and I_w, I_q are the cross-flow integrals

$$I_w = C_D \int_{\text{tail}}^{\text{nose}} b(x)(w - xq)\,|w - xq|\,dx \tag{24}$$

$$I_q = C_D \int_{\text{tail}}^{\text{nose}} b(x)(w - xq)\,|w - xq|\,x\,dx \tag{25}$$

The system of equations (21) through (23) is written in the compact form

$$\dot{\mathbf{x}} = \mathbf{A}\mathbf{x} + \mathbf{g}(\mathbf{x}) \tag{26}$$

where

$$\mathbf{x} = [\theta, w, q] \tag{27}$$

is the three state variables vector, and $\mathbf{A}$ is the linearized system matrix evaluated at the nominal point $\mathbf{x}_0$. The term $\mathbf{g}(\mathbf{x})$ contains all nonlinear terms of the equations. Hopf bifurcation analysis can be performed by isolating the primary nonlinear term in $\mathbf{g}(\mathbf{x})$. Keeping terms up to third order, we can write

$$\mathbf{g}(\mathbf{x}) = \mathbf{g}^{(2)}(\mathbf{x}) + \mathbf{g}^{(3)}(\mathbf{x}) \tag{28}$$

Using equations (21) through (25), the various terms in (28) can be written as

$$\begin{aligned}
g_1^{(2)} &= 0 \\
g_2^{(2)} &= (I_y - M_{\dot{q}})mz_Gq^2 - (mx_G + Z_{\dot{q}})mz_Gwq + d_w^{(2)}(w,q) \\
g_3^{(2)} &= -(m - Z_{\dot{w}})mz_Gwq + (mx_G + M_{\dot{w}})mz_Gq^2 + d_q^{(2)}(w,q)
\end{aligned} \tag{29}$$

and

$$\begin{aligned}
g_1^{(3)} &= 0 \\
g_2^{(3)} &= d_w^{(3)}(w,q) + \tfrac{1}{6}a_{13}(x_{GB}\sin\theta_0 - z_{GB}\cos\theta_0)\theta^3 \\
g_3^{(3)} &= d_q^{(3)}(w,q) + \tfrac{1}{6}a_{23}(x_{GB}\sin\theta_0 - z_{GB}\cos\theta_0)\theta^3
\end{aligned} \tag{30}$$

Expansion in Taylor series of d_w, d_q requires expansion of the cross-flow integrals I_w, I_q, which require the Taylor series of

$$f(\xi) = \xi\,|\xi| \tag{31}$$

This expression can be converted into an analytic function using Dalzell's (1978) approximation

$$\xi\,|\xi| \approx \frac{5}{16}\xi_c\xi + \frac{35\xi^3}{48\xi_c} \tag{32}$$

which is derived by a least-squares fit of an odd series over some assumed range of ξ, namely $-\xi_c < \xi < \xi_c$. This approximation, which is shown in Fig. 3, has been extensively used in ship roll motion studies and is very useful for its intended purpose. However, in the present problem it suffers from several major drawbacks:

- It introduces a linear term which depends on the assumed range of motion, and it renders the critical speed a function of the vehicle motions.
- The cubic term, which is ultimately responsible for the Hopf bifurcation analysis, is a function of the assumed range of vehicle motions which cannot be known in advance.

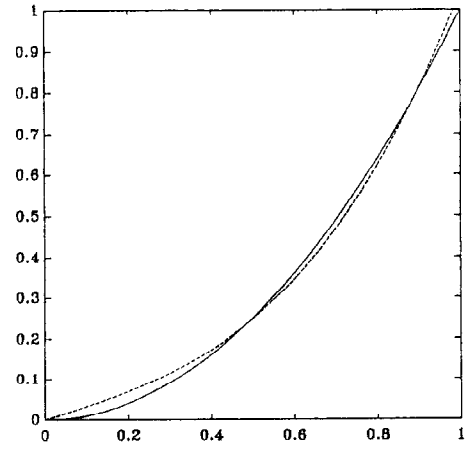

Fig. 3 Graphical representation of Dalzell's approximation of $\xi|\xi|$ versus ξ/ξ_c. Solid curve is the exact expression and dotted curve is the approximation (32)

- As Fig. 3 demonstrates, the slope of the actual curve at the origin is significantly different than the approximation, which would make the bifurcation results unreliable.

Instead of Dalzell's approximation, we employ the concept of generalized gradient (Clarke 1983), which is used in the study of control systems involving discontinuous or non-smooth functions. In this way we approximate the gradient of a non-smooth function at a discontinuity by a map equal to the convex closure of the limiting gradients near the discontinuity. In our problem we write

$$f(\xi) = \xi_0|\xi_0| + 2|\xi_0|(\xi - \xi_0) + \text{sign}(\xi_0)(\xi - \xi_0)^2 + f^{(3)}(\xi) \quad (33)$$

as the Taylor series expansion of $f(\xi)$ near ξ_0. The sign function in (33) can be approximated by

$$\text{sign}(\xi_0) = \lim_{\gamma \to 0} \tanh\left(\frac{\xi_0}{\gamma}\right) \quad (34)$$

A graphical representation of the approximation (34) is shown in Fig. 4. The quantity γ is a small regularization parameter and is used for proper normalization of the results. Using (34), we can approximate $f(\xi)$ in the vicinity of $\xi_0 = 0$ by

$$\xi|\xi| \approx \frac{1}{6\gamma}\xi^3 \quad (35)$$

Since

$$\xi \mapsto w - xq \quad (36)$$

we can express the non-smooth cross-flow integral terms by

$$I_w = \frac{C_D}{6\gamma}(E_0 w^3 - 3E_1 w^2 q + 3E_2 w q^2 - E_3 q^3) \quad (37)$$

$$I_q = \frac{C_D}{6\gamma}(E_1 w^3 - 3E_2 w^2 q + 3E_3 w q^2 - E_4 q^3) \quad (38)$$

where

$$E_i = \int_{\text{tail}}^{\text{nose}} x^i b(x) dx \quad (39)$$

are the moments of the vehicle "waterplane" area.

Using the previous second- and third-order Taylor series expansions, equation (26) is written in the form

$$\dot{\mathbf{x}} = \mathbf{A}\mathbf{x} + \mathbf{g}^{(2)}(\mathbf{x}) + \mathbf{g}^{(3)}(\mathbf{x}) \quad (40)$$

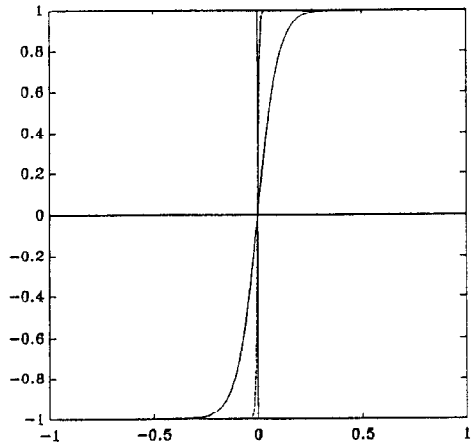

Fig. 4 Graphical representation of sign function and its hyperbolic tangent approximation (34). Solid curve corresponds to $\gamma = 0.1$ and dotted curve to $\gamma = 0.01$

If $\mathbf{T}$ is the matrix of eigenvectors of $\mathbf{A}$ evaluated at the critical point $u = u_c$, the linear change of coordinates

$$\mathbf{x} = \mathbf{T}\mathbf{z},\ \mathbf{z} = \mathbf{T}^{-1}\mathbf{x} \quad (41)$$

transforms system (40) into its normal coordinate form

$$\dot{\mathbf{z}} = \mathbf{T}^{-1}\mathbf{A}\mathbf{T}\mathbf{z} + \mathbf{T}^{-1}\mathbf{g}^{(2)}(\mathbf{T}\mathbf{z}) + \mathbf{T}^{-1}\mathbf{g}^{(3)}(\mathbf{T}\mathbf{z}) \quad (42)$$

At the Hopf bifurcation point, matrix $\mathbf{T}^{-1}\mathbf{A}\mathbf{T}$ takes the form

$$\mathbf{T}^{-1}\mathbf{A}\mathbf{T} = \begin{bmatrix} 0 & -\omega_0 & 0 \\ \omega_0 & 0 & 0 \\ 0 & 0 & p \end{bmatrix}$$

where ω_0 is the imaginary part of the critical pair of eigenvalues, and the remaining eigenvalue p is negative. For values of u close to the bifurcation point u_c, matrix $\mathbf{T}^{-1}\mathbf{A}\mathbf{T}$ becomes

$$\mathbf{T}^{-1}\mathbf{A}\mathbf{T} = \begin{bmatrix} \alpha'\epsilon & -(\omega_0 + \omega'\epsilon) & 0 \\ (\omega_0 + \omega'\epsilon) & \alpha'\epsilon & 0 \\ 0 & 0 & p + p'\epsilon \end{bmatrix}$$

where ϵ denotes the criticality difference

$$\epsilon = u - u_c \quad (43)$$

and

α' = derivative of the real part of the critical eigenvalue with respect to ϵ
ω' = derivative of the imaginary part of the critical eigenvalue with respect to ϵ
p' = derivative of p with respect to ϵ

Due to continuity, the eigenvalue $p + p'\epsilon$ remains negative for small nonzero values of ϵ. Therefore, the coordinate z_3 corresponds to a negative eigenvalue and is asymptotically stable. Center manifold theory predicts that the relationship between the critical coordinates z_1, z_2 and the stable coordinate z_3 is at least quadratic order. We can then write z_3 as

$$z_3 = \alpha_{11}z_1^2 + \alpha_{12}z_1z_2 + \alpha_{22}z_2^2 \quad (44)$$

where the coefficients α_{ij} in the quadratic center manifold expansion (44) need to be determined. By differentiating equation (44) we obtain

$$\dot{z}_3 = 2\alpha_{11}z_1\dot{z}_1 + \alpha_{12}(\dot{z}_1z_2 + z_1\dot{z}_2) + 2\alpha_{22}z_2\dot{z}_2 \quad (45)$$

We substitute $\dot{z}_1 = -\omega_0 z_2$ and $\dot{z}_2 = \omega_0 z_1$ from equation (42) into (45), and we obtain

$$\dot{z}_3 = \alpha_{12}\omega_0 z_1^2 + 2(\alpha_{22} - \alpha_{11})\omega_0 z_1 z_2 - \alpha_{12}\omega_0 z_2^2 \quad (46)$$

The third equation of (42) is written as

$$\dot{z}_3 = pz_3 + [\mathbf{T}^{-1}\mathbf{g}^{(2)}(\mathbf{T}\mathbf{z})]_{(3,3)} \quad (47)$$

where terms up to second order have been kept. If we denote the elements of $\mathbf{T}$ and $\mathbf{T}^{-1}$ by

$$\mathbf{T} = [m_{ij}],\ \mathbf{T}^{-1} = [n_{ij}] \quad (48)$$

then

$$\mathbf{T}^{-1}\mathbf{g}^{(2)}(\mathbf{T}\mathbf{z}) = \begin{bmatrix} d_1 \\ d_2 \\ d_3 \end{bmatrix}$$

where

$$d_1 = n_{12}(\ell_{25}z_1^2 + \ell_{26}z_1z_2 + \ell_{27}z_2^2) + n_{13}(\ell_{35}z_1^2 + \ell_{36}z_1z_2 + \ell_{37}z_2^2) \quad (49)$$

$$d_2 = n_{22}(\ell_{25}z_1^2 + \ell_{26}z_1z_2 + \ell_{27}z_2^2) + n_{23}(\ell_{35}z_1^2 + \ell_{36}z_1z_2 + \ell_{37}z_2^2 \quad (50)$$

$$d_3 = n_{32}(\ell_{25}z_1^2 + \ell_{26}z_1z_2 + \ell_{27}z_2^2) + n_{33}(\ell_{35}z_1^2 + \ell_{36}z_1z_2 + \ell_{37}z_2^2) \quad (51)$$

Expression for the coefficients ℓ_{ij} are given in Papadimitriou (1994).

Equation (47) then becomes

$$\dot{z}_3 = pz_3 + d_3 \quad (52)$$

and substituting (44) and (51) into (52) we get

$$\dot{z}_3 = (p\alpha_{11} + n_{32}\ell_{25} + n_{33}\ell_{35})z_1^2 + (p\alpha_{12} + n_{32}\ell_{26} + n_{33}\ell_{36})z_1z_2 + (p\alpha_{22} + n_{32}\ell_{27} + n_{33}\ell_{37})z_2^2 \quad (53)$$

Comparing coefficients of (46) and (53) we get

$$-p\alpha_{11} + \omega_0\alpha_{12} = n_{32}\ell_{25} + n_{33}\ell_{35} \quad (54)$$

$$-2\omega_0\alpha_{11} - p\alpha_{12} + 2\omega_0\alpha_{22} = n_{32}\ell_{26} + n_{33}\ell_{36} \quad (55)$$

$$-\omega_0\alpha_{12} - p\alpha_{22} = n_{32}\ell_{27} + n_{33}\ell_{37} \quad (56)$$

Solution of the system of linear equations (54) through (56) yields the coefficients in the center manifold expansion (44).

Using the previous Taylor expansions and center manifold approximations, we can write the reduced two-dimensional system that describes the center manifold flow of (42) in the form,

$$\dot{z}_1 = \alpha'\epsilon z_1 - (\omega_0 + \omega'\epsilon)z_2 + F_1(z_1,z_2) \quad (57)$$

$$\dot{z}_2 = (\omega_0 + \omega'\epsilon)z_1 + \alpha'\epsilon z_2 + F_2(z_1,z_2) \quad (58)$$

where

$$F_1(z_1z_2) = r_{11}z_1^3 + r_{12}z_1^2z_2 + r_{13}z_1z_2^2 + r_{14}z_2^3 + p_{11}z_1^2 + p_{12}z_1z_2 + p_{13}z_2^2 \quad (59)$$

$$F_2(z_1z_2) = r_{21}z_1^3 + r_{22}z_1^2z_2 + r_{23}z_1z_2^2 + r_{24}z_2^3 + p_{21}z_1^2 + p_{22}z_1z_2 + p_{23}z_2^2 \quad (60)$$

and

$$r_{ij} = n_{i2}\ell_{2j} + n_{i3}\ell_{3j}, \quad i = 1,2, \quad j = 1, \ldots, 4 \quad (61)$$

$$p_{ij} = n_{i2}\ell_{2k} + n_{i3}\ell_{3k}, \quad i = 1,2, \quad j = 1,2,3, \quad k = j + 4 \quad (62)$$

If we introduce polar coordinates in the form

$$z_1 = R\cos\phi, \; z_2 = R\sin\phi \quad (63)$$

we can use (57) and (58) to produce an equation describing the rate of change of the radial coordinate R

$$\dot{R} = \alpha'\epsilon R + P(\phi)R^3 + Q(\phi)R^2 \quad (64)$$

This equation contains one variable, R, which is slowly varying in time, and another variable, ϕ, which is a fast variable. Therefore, equation (64) can be averaged over one complete cycle in ϕ to produce an equation with constant coefficients and similar stability properties

$$\dot{R} = \alpha'\epsilon R + KR^3 + LR^2 \quad (65)$$

where

$$K = \frac{1}{2\pi}\int_0^{2\pi} P(\phi)d\phi = \frac{1}{8}(3r_{11} + r_{13} + r_{22} + 3r_{24}) \quad (66)$$

$$L = \frac{1}{2\pi}\int_0^{2\pi} Q(\phi)d\phi = 0 \quad (67)$$

Therefore, the averaged equation (65) becomes

$$\dot{R} = \alpha'\epsilon R = KR^3 \quad (68)$$

Equation (68) admits two steady-state solutions, one at $R = 0$ which corresponds to the trivial equilibrium solution at zero, and one at

$$R_0 = \sqrt{-\frac{\alpha'}{K}\epsilon} \quad (69)$$

This equilibrium solution corresponds to a periodic solution or limit cycle in the cartesian coordinates z_1, z_2. For this limit cycle to exist, the quantity R_0 must be a real number. In our case α' is always positive, since the system loses its stability; i.e., the real part of the critical pair of eigenvalues changes from negative to positive, for increasing u. Therefore, existence of these periodic solutions depends on the value of K. Specifically

- if $K < 0$, periodic solutions exist for $\epsilon > 0$ or $u > u_c$, and
- if $K > 0$, periodic solutions exist for $\epsilon < 0$ or $u < u_c$.

The characteristic root of (68) in the vicinity of (69) is

$$\beta = -2\alpha'\epsilon \quad (70)$$

and we can see that

- if periodic solutions exist for $u > u_c$ they are stable, and
- if periodic solutions exist for $u < u_c$ they are unstable.

The period of these periodic solutions can be estimated as follows. Equations (57), (58), and (63) produce an equation in $\dot{\phi}$ similar to (64)

$$\dot{\phi} = \omega_0 + \omega'\epsilon + F(\phi)R^2 + G(\phi)R \quad (71)$$

The averaged form of (71) is

$$\dot{\Phi} = \omega_0 + \omega'\epsilon + MR^2 \quad (72)$$

where

$$M = \frac{1}{2\pi}\int_0^{2\pi} F(\phi)d\phi = \frac{1}{8}(3r_{11} + r_{23} - r_{12} - 3r_{14}) \quad (73)$$

The limit cycle period can be computed by substituting (69) into (72)

$$T = \frac{2\pi}{\omega_0 + \omega'\epsilon + MR_0^2} = \frac{2\pi}{\omega_0}\left(1 - \frac{\omega'K - \alpha'M}{\omega_0 K}\epsilon\right) + O(\epsilon^2) \quad (74)$$

Results and discussion

Typical results of the nonlinear stability coefficient K are shown in Figs. 5 and 6. Figure 5 presents a plot of $K \cdot \gamma$ versus x_G for $z_G = 0.015$ and for different values of C_D. It should be emphasized that the use of $K \cdot \gamma$ is more meaningful than the use of K, since it properly accounts for the use of the regularization parameter γ as seen from equations (35) and (68). Numerical evidence demonstrates that all curves $K \cdot \gamma$ versus x_G converge for $\gamma \to 0$. For practical purposes, values of γ smaller than 0.001 produce identical results. The results of Fig. 5 demonstrate the profound effect that the quadratic drag coefficient C_D has on stability of limit cycles. All Hopf bifurcations are supercritical ($K < 0$), and they become stronger supercritical as C_D is increased. It is worth noting that results for $C_D = 0$ produce subcritical behavior, $K > 0$, which is clearly incorrect. Thus, neglecting the effects of C_D would have produced entirely wrong results in the present problem. Figure 6 shows a plot of $K \cdot \gamma$ versus x_G for $C_D = 0.5$ and different values of the metacentric height z_G. It can be seen that, the bifurcations become stronger supercritical as initial stability z_G is increased.

The bifurcation analysis results are verified by direct numerical simulations shown in Figs. 7 through 9. Figure 7 shows the results of two numerical simulations for two val-

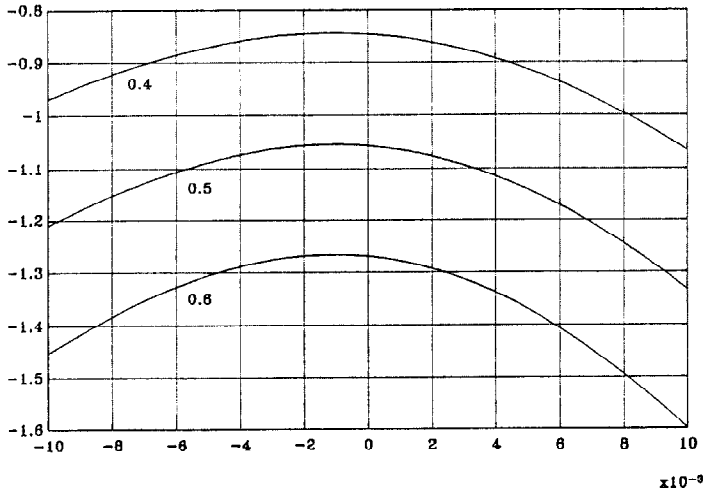

Fig. 5 $K \cdot \gamma$ versus x_G for $z_G = 0.015$ and different values of drag coefficient C_D

ues of nominal speed u_0 in terms of the vehicle pitch angle θ (in degrees) versus time (in seconds). The critical value of speed, u_c, is about 0.495 as can be seen from Fig. 2, while the other parameters in the simulations were $C_D = 0.5$, $z_G = 0.015$, and $x_G = 0$. It can be seen that convergence to zero is ensured for $u_0 < u_c$ and convergence to a limit cycle occurs for $u_0 > u_c$. This indicates supercritical behavior as shown before. A selection of time histories is shown in Fig. 8 for a range of forward speeds and the same parameters as in Fig. 7. The same initial disturbance, $\theta = 5$ deg, was introduced at $t = 0$ for all simulations. It can be seen that the amplitude of limit cycles increases as the distance of u from u_c is increasing. The rate of convergence of solutions to their limit cycles is also increasing, while their period remains essentially constant. These results are summarized in Fig. 9, where the amplitudes of the numerically computed limit cycles are plotted versus u_0 The behavior is clearly supercritical, which agrees with our findings of the bifurcation analysis.

Bias effects

Loss of stability

Stability analysis of motions at a nonzero angle of attack can be performed by first introducing some bias into the steady-state solution and its perturbations. This can be achieved by maintaining a nonzero dive plane angle. In this case the steady-state solutions are $q_0 = 0$, and w_0, θ_0 are computed from

$$Z_w w_0 - C_D E_0 w_0 |w_0| + Z_\delta \delta = 0 \tag{75}$$

$$M_w w_0 + C_D E_1 w_0 |w_0| - W(x_{GB}\cos\theta_0 + z_{GB}\sin\theta_0) + M_\delta \delta = 0 \tag{76}$$

The coefficients E_0, E_1 are computed from (39). In order to solve (75) we observe that when $\delta > 0$, then $w_0 < 0$

$$w_0 = \frac{-Z_w - \sqrt{Z_w^2 - 4C_D E_0 Z_\delta \delta}}{-2C_D E_0} \tag{77}$$

and when $\delta < 0$, then $w_0 > 0$

$$w_0 = \frac{-Z_w - \sqrt{Z_w^2 + 4C_D E_0 Z_\delta \delta}}{-2C_D E_0} \tag{78}$$

The angle θ_0 can then be computed from equation (76).

Linearization of the equations of motion in the neighborhood of the above equilibrium point produces the linear system

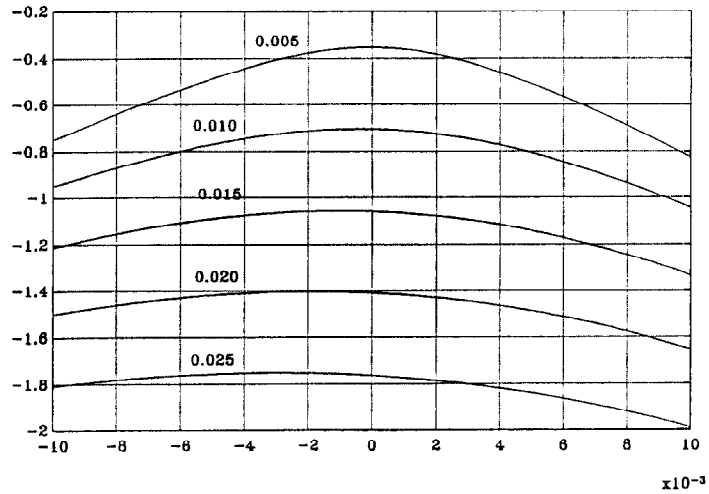

Fig. 6 $K \cdot \gamma$ versus x_G for $C_D = 0.5$ and different values of metacentric height z_G

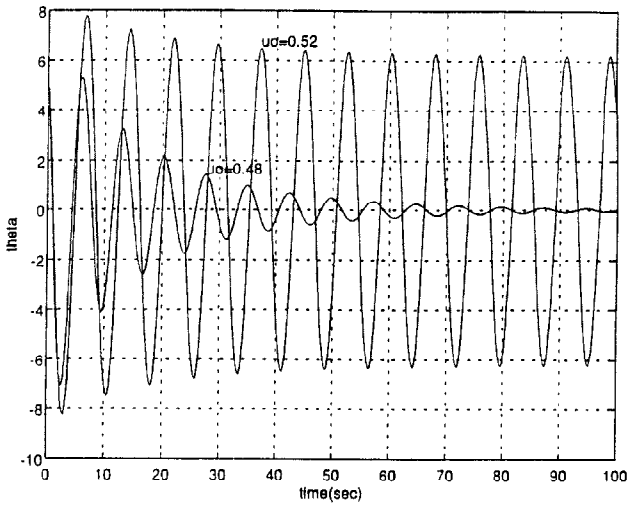

Fig. 7 Time histories (θ,t) for $C_D = 0.5$, $z_G = 0.015$, $x_G = 0$, and two different values of nominal speed

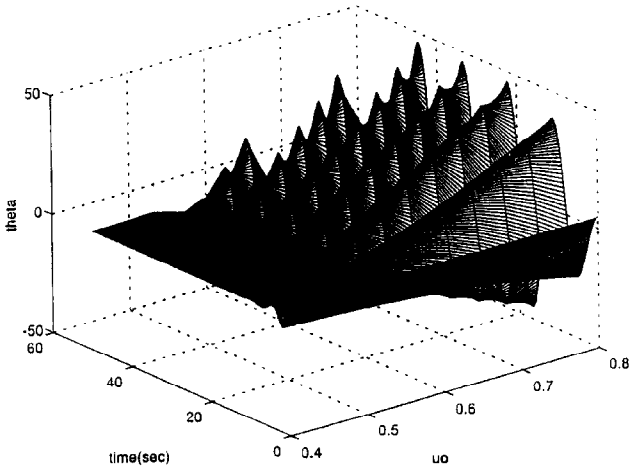

Fig. 8 Time histories (θ,t) for $C_D = 0.5$, $z_G = 0.015$, $x_G = 0$, and a range of nominal forward speeds

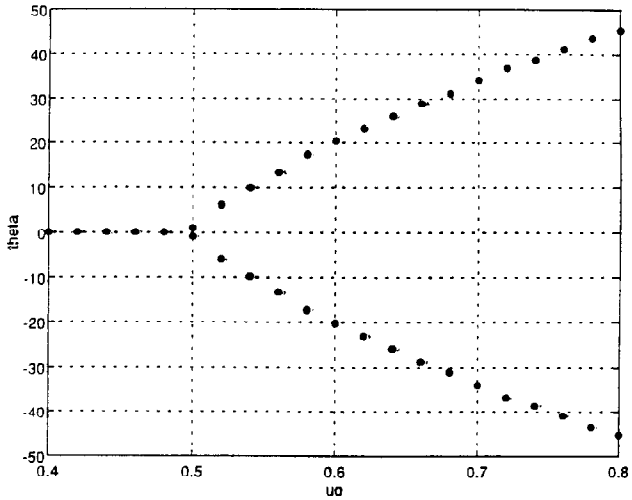

Fig. 9 Limit cycle amplitudes from results of Fig. 8

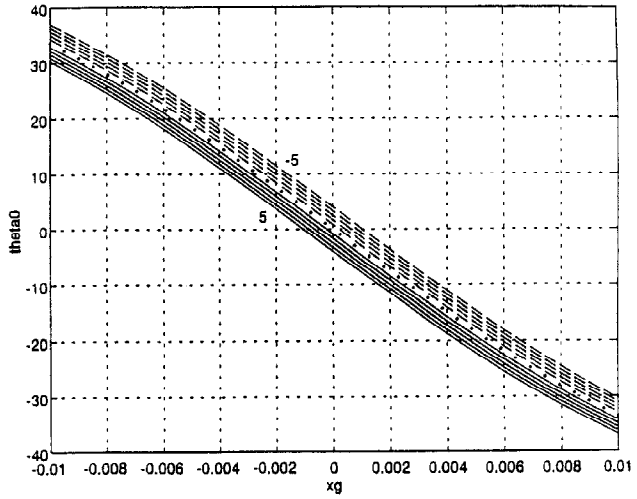

Fig. 10 Pitch angle θ_0 versus x_G for $z_G = 0.015$, $u_0 = 0.5$, and different values of δ

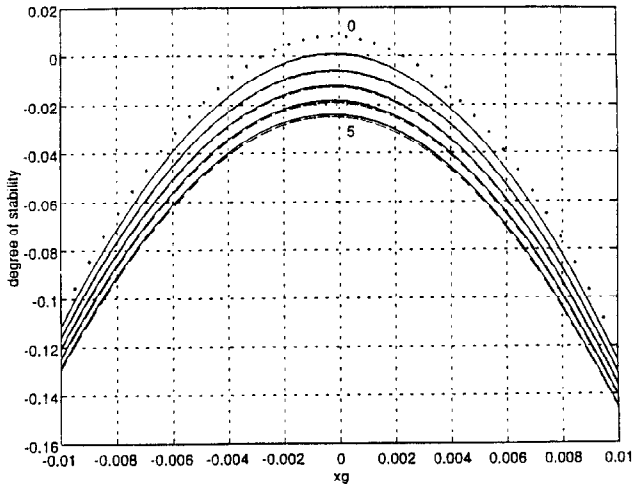

Fig. 11 Degree of stability versus x_G for $z_G = 0.015$, $u_0 = 0.5$, and different values of δ

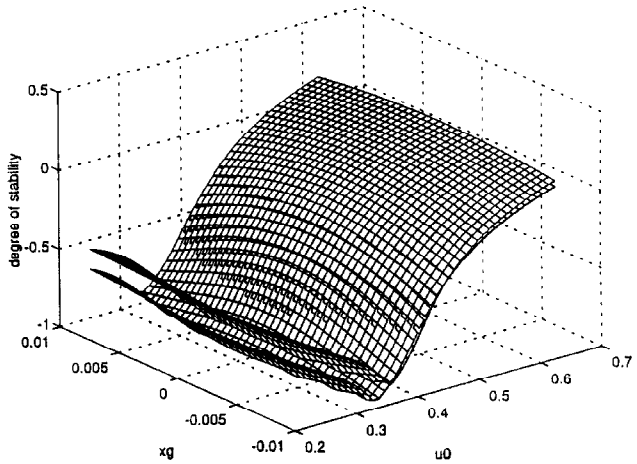

Fig. 12 Degree of stability versus x_G and u_0 for $z_G = 0.015$ and two values of δ

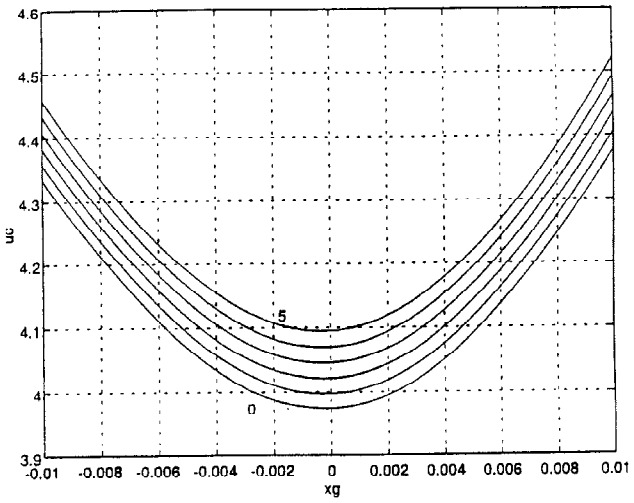

Fig. 13 Critical speed u_c versus x_G for $z_G = 0.015$ and different values of δ

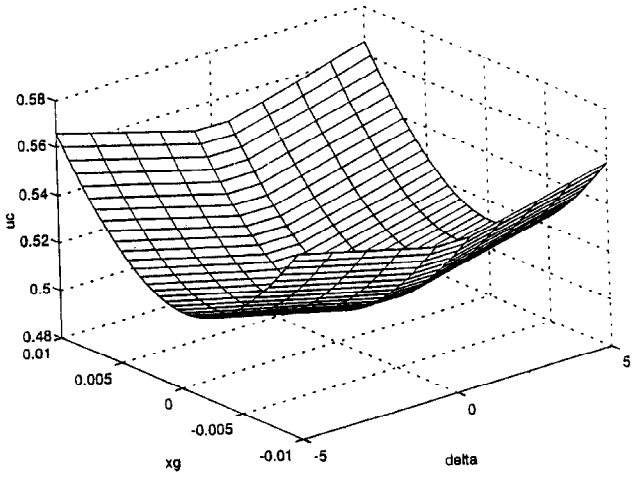

Fig. 14 Critical speed u_c versus x_G and δ for $z_G = 0.015$

$$(m - Z_{\dot{w}})\dot{w} - (mx_G + Z_{\dot{q}})\dot{q} = (Z_w - 2C_D E_0 |w_0|)w + (Z_q + m + 2C_D E_1 |w_0|)q \quad (79)$$

$$-(M_{\dot{w}} + mx_G)\dot{w} + (I_y + M_{\dot{q}})\dot{q} = (M_w + 2C_D E_1 |w_0|)w + (M_q - mx_G - mz_G w_0 - 2C_D E_2 |w_0|)q + W(x_{GB}\sin\theta_0 - z_{GB}\cos\theta_0)\theta \quad (80)$$

$$\dot{\theta} = q \quad (81)$$

where the variables w, θ are understood as small deviations from their equilibrium values. Numerical solution of the generalized eigenvalue problem (79) and (81) yields the critical speed values where the nominal equilibrium solution becomes unstable.

Analysis of Hopf bifurcations

It can be numerically verified that the above calculations for the new critical speed result in a loss of stability in the form of Hopf bifurcations, as for the $\delta = 0$ case. These Hopf bifurcations can be analyzed using the same general methodology that was developed in the previous section. The nonlinear expansions are like equations (21) to (23) with the following changes: The substitutions

$$Z_w \to Z_w - 2C_D E_0 w_0$$

$$M_w \to M_w + 2C_D E_1 w_0$$

$$Z_q + m \to Z_q + m + 2C_D E_1 w_0$$

$$M_q - mx_G \to M_q - mx_G - mz_G w_0 - 2C_D E_2 w_0$$

are assumed in the definition of coefficients α_{ij}. Furthermore, equation (33) produces second-order contributions due to $w_0 \neq 0$, as well as a third order. Using (33) we can compute the second-order expansions of $d_w^{(2)}$ and $d_q^{(2)}$ in (29) using

$$I_w^{(2)} = C_D(E_0 w^2 - 2E_1 wq + E_2 q^2) \quad (82)$$

$$I_q^{(2)} = C_D(E_1 w^2 - 2E_2 wq + E_3 q^2) \quad (83)$$

These equations are valid for $w_0 > 0$ or $\delta < 0$. For $\delta > 0$ the signs of E_i must be switched. The third-order expansions $I_w^{(3)}$ and $I_q^{(3)}$ are the same as in equations (37) and (38). Using these additional terms, the nonlinear stability coefficient K can be computed in the same way as in the previous section.

Results and discussion

Typical results for $\delta \neq 0$ are shown in Figs. 10 through 15. Figure 10 shows the equilibrium pitch under θ_0 (in degrees)

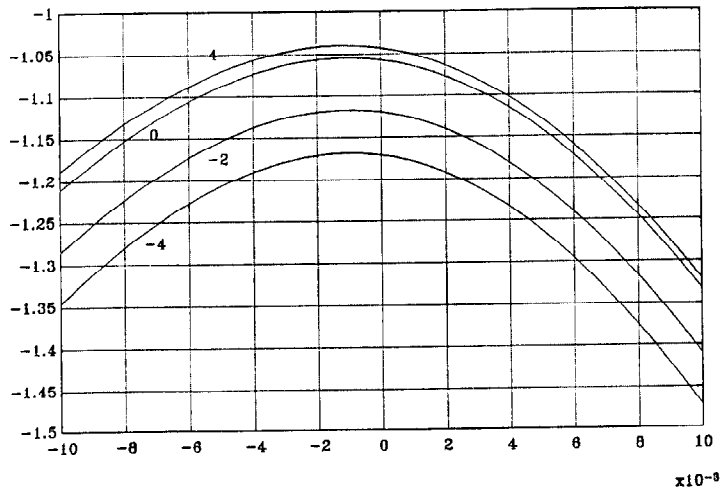

Fig. 15 Nonlinear stability coefficient K versus x_G for $C_D = 0.5$, $z_G = 0.015$, and different values of δ

versus x_G for different values of δ from -5 to 5 deg with increments of 1 deg. Solid curves correspond to positive δ and dashed curves to negative. Figure 11 shows the degree of stability for the equilibrium points of Fig. 10, while Fig. 12 presents the degree of stability in a three-dimensional view. It can be seen that positive and negative values of δ have almost identical stability characteristics. Furthermore, the degree of stability becomes more negative as the absolute value of δ is increased, which means that we expect a wider domain of stability in this case. This is verified by the critical speed plots shown in Figs. 13 and 14. The critical speed is minimum for $\delta = 0$ and it increases monotonically with increasing absolute value of δ. This stabilizing effect of asymmetry (bias) remains approximately true for the nonlinear analysis, as demonstrated by the results of Fig. 15. It can be seen that the nonlinear stability coefficient K becomes more negative as δ is decreasing from zero. For increasing δ, K becomes less negative but the difference from the $\delta = 0$ calculations appears to be very small. Therefore, limit cycle stability is not significantly affected by the bias effects that are induced by small nonzero dive plane angles.

5. Concluding remarks

This work presented a comprehensive nonlinear study of straight-line stability of motion of submersibles in the dive plane under open-loop conditions. A systematic perturbation analysis demonstrated that the effects of surge in heave/pitch are small and can be neglected. Primary loss of stability was shown to occur in the form of Hopf bifurcations to periodic solutions. The critical speed where instability occurs was computed in terms of metacentric height, longitudinal separation of the centers of buoyancy and gravity, and the dive plane angle. Analysis of the periodic solutions that resulted from the Hopf bifurcations was accomplished through Taylor expansions, up to third order, of the equations of motion. A consistent approximation, utilizing the generalized gradient, was used to study the nonanalytic quadratic cross-flow integral drag terms. The main results of this study are summarized as follows:

1. The critical speed of loss of stability is a monotonically increasing function of both vertical and longitudinal LCG/LCB separation. This means that a vehicle which is stable when properly trimmed will remain stable for off-trim conditions.

2. Loss of stability occurs always in the form of supercritical Hopf bifurcations with the generation of stable limit cycles. It was found that this is mainly due to the stabilizing effects of the quadratic drag forces.

3. Even though the quadratic drag forces do not influence the initial loss of stability, they have a significant effect on post-loss of stability stabilization.

4. The critical speed is minimum for zero dive plane angles, and is monotonically increasing for nonzero angles. Limit cycle stability is not significantly affected by the bias effects that are induced by small nonzero dive plane angles.

It should be emphasized that the occurrence of supercritical Hopf bifurcations is an attribute of the open-loop system only. Under closed-loop control, it is possible to experience either supercritical or strongly subcritical Hopf bifurcations, as shown in Papoulias et al (1995). The latter are particularly severe in practice since self-sustained vehicle oscillations may be initiated prior to loss of stability, depending on the level of external excitation or the initial conditions.

Acknowledgments

The authors would like to recognize the financial support of the Naval Postgraduate School Direct Research Fund.

References

Arentzen, E. S. and Mandel, P. 1960 Naval architectural aspects of submarine design. *Trans. SNAME,* **68,** 662–692.

Bender, C. M. and Orszag, S. A. 1978 *Advanced Mathematical Methods for Scientists and Engineers,* McGraw-Hill, New York.

Chow, S.-N. and Mallet-Paret, J. 1977 Integral averaging and bifurcation. *Journal of Differential Equations,* **26,** 112–159.

Clayton, B. R. and Bishop, R. E. D. 1982 *Mechanics of Marine Vehicles,* Gulf Publishing Company, Houston.

Clarke, F. 1983 *Optimization and Nonsmooth Analysis,* Wiley, New York.

Dalzell, J. F. 1978 A note on the form of ship roll damping. Journal of Ship Research, **22,** 3, Sept.

Feldman, J. 1987 Straightline and rotating arm captive-model experiments to investigate the stability and control characteristics of submarines and other submerged vehicles. Carderock Division, Naval Surface Warfare Center, Report DTRC/SHD-0303-20.

Gertler, M. and Hagen, G. R. 1967 Standard equations of motion for submarine simulation. David Taylor Research Center Report 2510, Bethesda, Md.

Guckenheimer, J. and Holmes, P. 1983 *Nonlinear Oscillations, Dynamical Systems, and Bifurcations of Vector Fields,* Springer-Verlag, New York.

Hassard, B. and Wan, Y. H. 1978 Bifurcation formulae derived from center manifold theory. *Journal of Mathematical Analysis and Applications,* **63,** 297–312.

Papadimitriou, H. I. 1994 A nonlinear study of open loop dynamic stability of submersible vehicles in the dive plane. Master of Science in Mechanical Engineering and Mechanical Engineer's thesis, Naval Postgraduate School, Monterey, Calif.

Papoulias, F. A., Aydin, I., and McKinley, B. D. 1993 Characterization of steady state solutions of submarines under casualty conditions. In *Nonlinear Dynamics of Marine Vehicles,* J. M. Falzarano, F. A. Papoulias, Eds., ASME, New York.

Papoulias, F. A., Bateman, C. A., and Ornek, S. 1995 Dynamic loss of stability in depth control of submersible vehicles. *Journal of Applied Ocean Research,* in press.

Roddy, R. F. 1990 Investigation of the stability and control characteristics of several configurations of the DARPS SUBOFF model (DTRC model 5470) from captive-model experiments. Carderock Division, Naval Surface Warfare Center, Report DTRC/SHD-1298-08.

Smith, N. S., Crane, J. W., and Summey, D. C. 1978 SDV simulator hydrodynamic coefficients. Naval Coastal Systems Center, Report NCSC-TM231-78.

Tinker, S. J. 1978 Fluid memory effects on the trajectory of a submersible. *International Shipbuilding Progress,* **25,** 290.